EPSC Abstracts
Vol. 10, EPSC2015-91, 2015
European Planetary Science Congress 2015

Radiative transfer model for Solar System ices

F. Andrieu (1,2), F. Schmidt (1,2) , S. Douté (3), B. Schmitt (3) and O. Brissaud (3)

(1) Univ Paris-Sud, Laboratoire GEOPS, Orasy, France (2) CNRS, Orsay, F-91405 (3) Institut de Planétologie et d'Astrophysique de Grenoble, CNRS-Univ. Joseph Fourier, France (francois.andrieu@u-psud.fr)

Abstract

We developed a radiative transfer model [1] that simulates the bidirectional reflectance of a contaminated slab layer of ice overlaying a granular medium, under geometrical optics conditions. Designed for planetary studies, this model has a fast computer implementation and thus is suitable for planetary high spatial/spectral resolution hyperspectral data analysis. We will present here its principles, its numerical and experimental validations and its possible applications.

1. Introduction

Ices are present in large amounts throughout the Solar System, on Earth, Mars, Europa, Triton and many other bodies. Their study is often a key to understand the planet's climate or history. Spectral unmixing has been proven a powerful technique to detect species, but cannot be trusted in quantitative analysis. Only radiative transfer models will provide quantitative analysis of the surface properties. Reflectance models for granular materials have already been developed [2,3]. However compact polycrystalline ices have been recognized to exist on several objects, CO_2 on Mars, N_2 on Triton and Pluto, owing to the very long light path-lengths measured, over several decimeters.We thus decided to develop a model designed to study contaminated ice slabs that was lacking in the literature in the goal to analyze spectro-imaging planetary data of these surfaces.

2. Model

The model [1] is inspired form an existing one [3] designed for granular media. We adapted it to compact structures. We suppose a layer of slab ice, containing various kind of impurities, overlaying an optically thick layer of granular material, as shown on figure 1. The roughness distribution of the surface is described as Gaussian using the mean slope angle θ, proposed by Hapke [2]. The ice matrix is described by its optical constants and its thickness. The inclusions are supposed to be close to spherical and of any other type than the matrix. It can be any type of other ice, mineral or even bubbles. We also suppose that they are homogeneously distributed in the slab.

The simulated bidirectional reflectance is the sum of a specular and a diffuse contributions. To estimate the specular contribution, we suppose that the surface is constituted of many unresolved facets. The orientations of these facets follow a probability density function determined by the roughness parameter. We integrate the various reflexions on every facet. The diffuse reflexion is estimated solving the radiative transfer equation under several hypothesis. We suppose (i) that the geometrical optics are respected. This means that the inclusions must be larger than the considered wavelength. We consider that the surface is illuminated by a collimated radiation (*e.g.* : Solar radiation). (ii) The first transit in the slab is considered collimated, but every following one is supposed isotropic due to rough granular substrate and scattering.

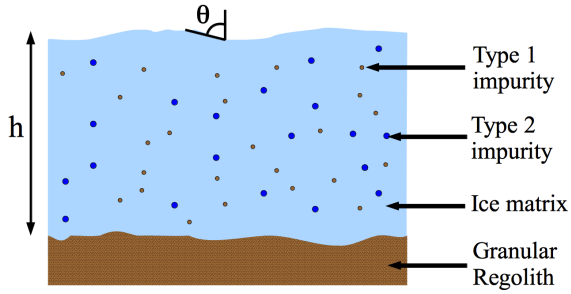

Figure 1: Scheme of the radiative transfer model.

3. Validations

We performed numerical and experimental validations on the model.

Numerical. We first checked the conservation of the energy at various points of the algorithm and showed that the model conserve the energy satisfactorily (more than 98% at the limits of the field of applicability). We will discuss the behavior of the model according to its parameters.

Experimental. We tested the model on real spectroscopic data [4]. Translucent synthetic water ice samples overlaying optically thick snow (from Arselle, in the French Alps) were measured in laboratory [5] at various geometries, inside and outside the specular spot. The model was able to reproduce correctly the data, and retrieve the parameters, as shown on figures 2 and 3. These results will be discussed thoroughly.

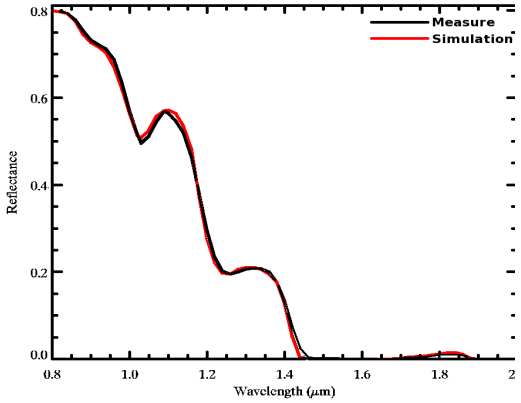

Figure 2: Measurement versus simulation for the reflectance of the first data sample. The estimated thickness of the slab (1.9 ± 0.5 mm) was consistently within the margin of uncertainties of the measurements (1.42 ± 0.3 mm).

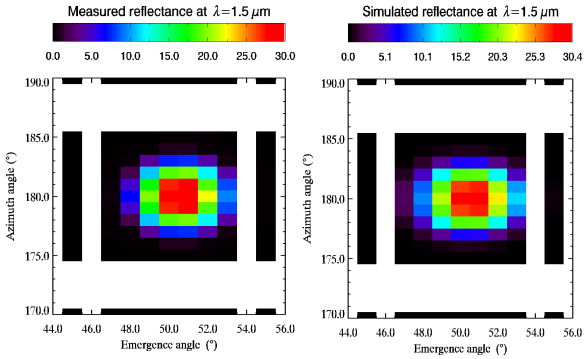

Figure 3 : Measure (left) versus simulation (right) for the specular spot at the 1.5 µm wavelength for a 50° incidence angle. The model reproduces correctly the shape as well as the level of reflectance in the specular lobe. The roughness parameter used for this simulation is very low (0.43°). That is consistent with the very flat surface described in the experiment.

5. Applications

The theoretical model does not depend on the type of material used. It is thus applicable to any matrix containing inclusions of any type. The fast implementation of the algorithm makes it suitable for massive hyperspectral data analysis. We will present a first example of application to planetary science with the case of seasonal evolution of the CO_2 ice cover on Mars. The study of other planetary bodies such as Pluto for example is also possible.

6. Conclusions and Perspectives

We developed [1] and validated [4] a radiative transfer model aiming at quantitatively studying planetary ices. This model has a fast implementation and is fully operational. It has a large field of application in the Solar System. We will start the planetary applications with the study of the Martian seasonal ice processes.

References

[1] Andrieu, F., Douté, S., Schmidt, F. and Schmitt, B., Radiative transfer model for contaminated rough slabs, JQSRT, *submitted*

[2] Hapke, B., Theory of Reflectance and Emittance Spectroscopy, Cambridge University Press, 2012

[3] Douté, S. and Schmitt B., A multilayer bidirectional reflectance model for the analysis of planetary surface hyperspectral images at visible and near-infrared wavelengths, J. Geophys. Res., 103(E13):31367-31389, 1998

[4] Andrieu, F., Douté, S., Schmidt, F., Schmitt, B. and Brissaud, O., A radiative transfer model for contaminated rough slabs: experimental validations, *in prep.*

[5] Brissaud, O., Schmitt, B., Bonnefoy, N., Douté, S., Rabou, P., Grundy, W. & Fily, M., Spectrogonio radiometer for the study of the bidirectional reflectance and polarization functions of planetary surfaces. 1. Design and tests, Appl. Opt., Applied Optics, OSA, 2004, 43, 1926-1937

EPSC Abstracts
Vol. 10, EPSC2015-331, 2015
European Planetary Science Congress 2015

Realistic uncertainties on Hapke model parameters from photometric measurements

F. Schmidt (1,2), J. Fernando (1,2,3)
(1) Univ. Paris-Sud, Laboratoire GEOPS, UMR8148, Orsay, F-91405 (2) CNRS, Orsay, F-91405 (3) at present time Laboratoire de Géologie de Lyon, Terre, Planètes, Environnement (Université de Lyon-Université Claude Bernard Lyon 1-CNRS-ENS Lyon, ERC eMars Team, 69622 Villeurbanne Cedex, France, (frederic.schmidt@@u-psud.fr)

Abstract

We propagate the uncertainties from the photometric measurement to the Hapke's photometric parameter using the Bayesian Monte Carlo approach. Since non-linearities are strong, uncertainties may have a non-Gaussian shape, especially in the case of relatively large uncertainties. We propose here to study synthetic examples in order to characterize the uncertainties of previous analysis but also to propose new strategies for new acquisition campaigns.

1. Introduction

The single particle phase function describes the manner in which an average element of a granular material diffuses the light in the angular space. Interestingly, this function is related to the particle properties, such surface roughness or internal scatterers. Usually, this function is approximated by the Henyey-Greenstein function with two parameters: the asymmetry parameter *b* describing the width of the scattering lobe and the backscattering fraction *c* describing the main direction of the scattering lobe. Hapke proposed a convenient analytical model to describe the spectro-photometry of granular materials [1]. This model has been widely used to interpret telescopic observations, remote sensing data, in situ and laboratory measurements [2,3]. Using a compilation of the published data, Hapke [4] recently studied the relationship of *b* and *c* for natural examples and proposed the hockey stick relation. For the moment, there is no theoretical explanation for this relationship. One goal of this project is to study a possible bias due to the retrieval method.

2. Method

We expand here an innovative Bayesian inversion method in order to study into detail the uncertainties of retrieved parameters (single scattering albedo, surface roughness, *b*, *c*, opposition effect) [5,6,7]. Indeed, the main advantage of this approach is that it provides all the possible solutions over the parameter domain through a probability density function (PDF). We performed sensitivity tests by mimicking various surface scattering properties and various single image-like/disk resolved image, Emission Phase Function (EPF)-like and Bidirectional Reflectance Distribution Function (BRDF)-like geometric sampling conditions under varied geometric conditions. Moreover, we estimated the favorable geometric conditions for an accurate estimation of photometric parameters in order to provide new constraints for future observation campaigns and instrumentations [8].

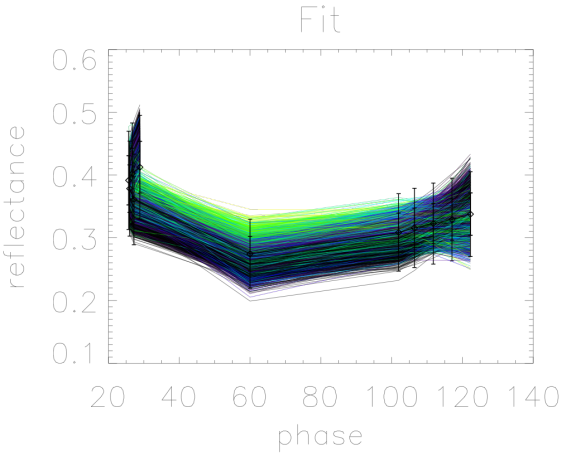

Figure 1: Example of a result on a synthetic observation with 10% uncertainty. The black curve represents the synthetic data with one and two standard deviations. Light color curves represent 500 sampled solutions from the Monte Carlo Markov Chain.

3. Results

As an example, we present in figures 1 to 3, the results for an estimation of the retrieved uncertainties in the following conditions: incidence=60° along the

azimuthal plane={30°; 210°} resulting to a phase angle range from 29° to 122°, and using the following model parameter set: ω=0.9, b=0.8, c=0.1, θ =15°, B0=1 and h=0. The uncertainty is set to 10% in REFF unit and independent for each geometry.

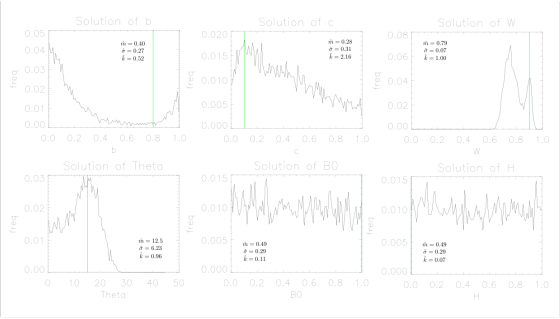

Figure 2: PDF of the solution, for each parameter of the Hapke's parameter on the same example as fig. 1. Each plot represents the histogram of the 500 solutions from the Monte Carlo Markov Chain. The color line represents the initial parameters set.

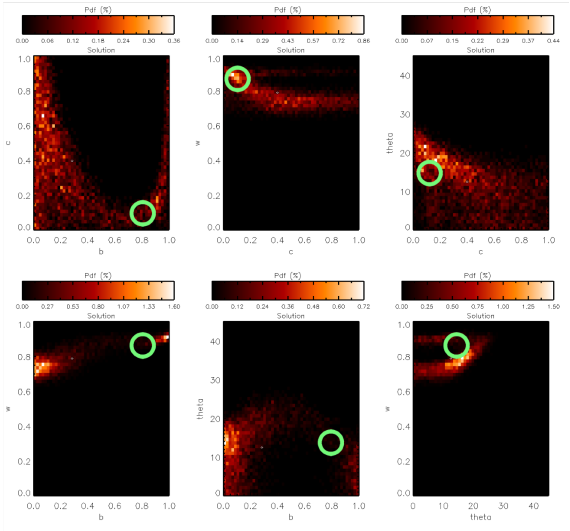

Figure 3: Probability Density Function (PDF) of the solution, for each couple of constrained parameters (ω, b, c, θ) on the same example as fig. 1 and 2. The black/white diamonds represent the average of the PDF. The green circles represent the expected values each parameter.

4. Summary and Conclusions

Some conclusions can be addressed [8]:

Non-linearities in the Hapke model are important leading to potential multiple solutions for EPF type measurements with at least data uncertainties larger than 5% and large azimuthal plane angle (> 30°).

One single EPF type observation with very favorable conditions (i.e., principal plane, incidence at 75°, emergence angle sampling up to 80°) is enough to constrain the parameters, even with data uncertainty level of 10%.

For data uncertainty less than 5% (for common spaceborne and laboratory measurements), the parameters can be estimated using single EPF, even with large uncertainties, under certain geometric configurations: close to the principal plane (azimuthal angle less than 45°) and high incidence angles (greater than 50°) leading to a broad phase angle range containing low and high phase angles to sufficiently describe the shape of the photometric curves).

On EPF data, we demonstrate that the uncertainties of the retrieved parameters follow the same hockey stick relation, suggesting that this relation is due to the fact that *b* and *c* are coupled parameters in the Hapke's model instead of natural phenomena. Nevertheless, the data used in the Hapke (2012) compilation generally are full BRDF which are not to be subject to this artifact.

References

[1] Hapke, Book, 1993

[2] Beck, P et al., 2012. Icarus 218 (1), 364–377.

[3] Johnson, J. R., et al., 2006 JGR, (E12), E12S16.

[4] Hapke, 2012, Icarus, 221, 1079-1083

[5] Ceamanos, X., et al.. 2013, JGR 118, 514–533.

[6] Fernando, J., et al, 2013. JGR, 118, 534–559.

[7] Fernando, J. et al., 2015. Icarus 253 (0), 271 – 295.

[8] Schmidt, F. and Fernando, J., Icarus, submitted

EPSC Abstracts
Vol. 10, EPSC2015-425, 2015
European Planetary Science Congress 2015

Wavelength dependence of spectro-photometric properties and link with the microtexture

C. Pilorget (1,2), J. Fernando (3,4,5), B.L. Ehlmann (1,6), F. Schmidt (3,4) and T. Hiroi (7)
(1) Division of Geological and Planetary Sciences, Caltech, Pasadena, CA 91125, USA, (2) Institut d'Astrophysique Spatiale, CNRS/Université Paris Sud, UMR8617, Orsay 91405, France, (3) Université Paris-Sud, GEOPS, UMR8148, Orsay 91405, France, (4) CNRS, Orsay 91405, France, (5) Laboratoire de Géologie de Lyon, Terre, Planètes, Environnement (Université de Lyon- Université Claude Bernard Lyon1-CNRS-ENS Lyon), ERC eMars Team, Villeurbanne Cedex, France (6) Jet Propulsion Laboratory, Caltech, Pasadena, CA 91109, USA, (7) Department of Earth, Environmental and Planetary Science, Brown University, Providence, RI 02912, USA (cedric.pilorget@ias.u-psud.fr)

Abstract

The surface scattered sunlight carries major information about the composition and microtexture of surface materials, thus enabling tracing back the geological and climatic processes that occurred on the planetary body. Here we perform laboratory spectro-goniometric measurements of different kinds of granular samples over the VIS-NIR spectral range, coupling the spectral and geometric dimensions to analyze their scattering behavior. To quantify the evolution of the scattering properties with the wavelength, we use an innovative inversion procedure based on a Bayesian approach to estimate photometric parameters from the Hapke model. The granular samples are also characterized by optical and SEM techniques in order to link these scattering variations with the grains' physical properties.

1. Introduction

As solar light penetrates into a surface, it is partially reflected back by interaction with its constituents and structures. The reflected signal exhibits variations with both the wavelength and the illumination/viewing geometry. In particular the spectral dimension (spectroscopy) of this signal gives constraints on the surface material composition through absorptions bands, whereas the geometric dimension (photometry) can be used to infer the surface material physical properties (e.g. grain size, shape, roughness, internal structure). Determining the grain microtexture is crucial and can be used as a tracer for identifying and characterizing the geological processes responsible for their formation and their evolution.
Numerous spaceborne and in situ missions have shown that the surfaces of planetary bodies in the Solar System exhibit some photometric variability, suggesting a diversity of material microtextures (e.g. [1,2]). To interpret these datasets, models have been developed to better understand how the grains' physical properties affect light scattering. Laboratory experiments have also been conducted on various samples (e.g. [3,4]) generally at one or a couple of wavelengths in the visible and/or very near-IR, similar to spaceborne acquisitions. Usually those datasets have been analyzed by using the Hapke model [5]. These different works have enabled to start some basic characterization of the surface microtexture, though uncertainties remain on how to translate these signal variations into unambiguous surface physical properties. In particular the question remains: to what extent do the different photometric parameters (absorptivity, phase function, macroscopic roughness) evolve over the full VIS-NIR spectral range (0.4-2.5 µm), commonly used in remote observations of planetary surfaces, and what is the link with the grains' microtexture and absorption properties?

2. Methodology

For this study, we analyzed the spectro-photometric properties of five different mineral samples with various chemical and physical properties: a basalt (from Medicine Lake Oregon [6]), an anhydrous basaltic glass (from the Big Island, Hawaii [6]), an olivine (from the San Carlos formation), a nontronite (Fe-rich smectite NG-1, obtained from the Clay Mineral Society) and a magnesite (Mg-carbonate, from Wards mineral supply). These five mineral samples were crushed and then sieved to limit the grain size to the 45-75 microns fraction. The granular samples were first analyzed with a binocular microscope, to characterize the physical properties at large scale and check the grain size distribution. The samples were then analyzed with a scanning electron

microscope (SEM) from the Caltech GPS Division Analytical Facility (e.g. Fig.1) to characterize the particles' structure down to the submicron scale. Their spectro-photometric properties were measured with the RELAB facility at Brown University [7] except for the olivine sample for which was used a manual spectro-goniometer setup developed at Caltech. The bidirectional reflectance was acquired at different geometries from 0.4 to 2.5 µm. The incidence angle was set to an intermediate value of 45 degrees and the bidirectionnal reflectance was measured in the principal plane at various emergence angles from -70 to +70 degrees. To quantify the evolution of the photometric behavior, we used the procedure developed by [8]. This methodology uses a Bayesian approach to estimate photometric parameters from the Hapke model. Four photometric parameters are obtained for each wavelength. Two parameters characterize the phase function of the grains (two-lobe Henyey-Greenstein phase function), another the grains single scattering albedo and the last one the macroscopic roughness. The final solution for each parameter is numerically sampled using a Monte Carlo Markov chain.

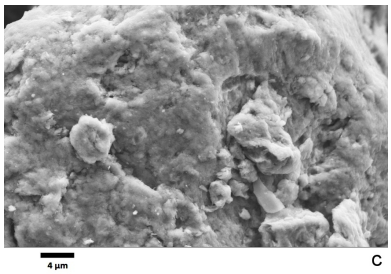

Figure 1: SEM image of the nontronite sample.

3. Results

Results have shown that for the derived photometric parameters, the single scattering albedo as expected, but also the phase function (through the asymmetry parameter b and the backscattering fraction c) and the macroscopic roughness, are wavelength dependent. In particular these can vary significantly over the VIS-NIR spectral range (e.g. Fig.2). The evolution of the photometric parameters with the wavelength appears to be a complex combination of multiple effects related to the grains physical properties (size, shape, roughness, transparency, etc.) and organization. Importantly, these photometric parameters are sensitive to the grains' external and internal structure at various scales from the grain scale down to the sub-micron one.

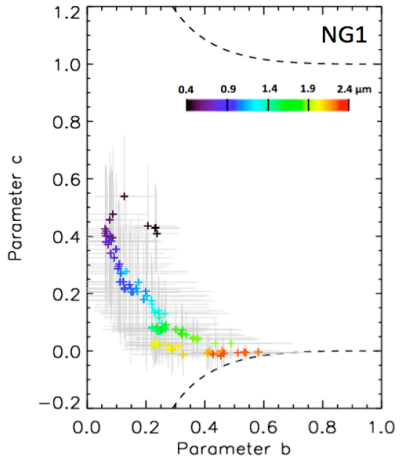

Figure 2: Evolution of nontronite sample phase function (through 2-lobe Henyey-Greenstein phase function parameters b and c) over the VIS-NIR spectral range. Here we represent the mean of the Probability Density Function. Only values of parameters b and c between the dashed upper and lower lines are allowed. Grey bars indicate the standard deviation around the mean of the PDF. Note that the mean is consistent with maximum of the PDF.

Acknowledgements

C.P and B.E acknowledge partial support from NNX14AG54G. C.P also acknowledges support from CNES and J.F support from the European Research Council under the European Union's Seventh Framework Program (FP7/2007-2013)/ERC Grant Agreement No. 280168. We also acknowledge NASA SSERVI program which supports RELAB operation.

References

[1] Sato H. et al. JGR (Planets) 119, Issue 8 1775-1805 (2014) [2] Fernando J. et al. Icarus 253, 271-295 (2015) [3] Shepard, M. K., Helfenstein, P. JGR (Planets) 112, 3001 (2007) [4] Souchon, A. L. et al. Icarus 215, 313-331 (2011) [5] Hapke B. (1993), [6] Wyatt, M. B. et al. JGR 106, 14711-14732 (2001) [7] Mustard, J. F., Pieters, C. M. JGR 94, 13619-13634 (1989) [8] Fernando, J. et al. JGR (Planets) 118, 534-559 (2013)

EPSC Abstracts
Vol. 10, EPSC2015-426, 2015
European Planetary Science Congress 2015

ICA applied to imaging spectroscopy remote sensing

S. Erard
LESIA, Observatoire de Paris/CNRS/UPMC/Univ. Paris-Diderot (stephane.erard@obspm.fr)

Abstract

A comparison of Principal Components Analysis and Independent Components Analysis is made in the context of imaging spectroscopy of the Solar System bodies. Specific behaviors are outlined and explained, using examples from recent space-borne experiments and telescopic observations. ICA is in general a much more efficient tool to analyze spectral data cubes.

1. Introduction

Imaging spectroscopy has become a major tool to study both the terrestrial environment and planetary surfaces and atmospheres. The data consists in 3D spectral cubes providing a reflectance spectrum of each pixel on the target, usually a small surface area. They provide limited resolution imaging but detailed spectral, and therefore compositional, information.

Altogether, spectral data cubes are very strongly correlated datasets in which significant compositional contrasts translate as small differences in variance. The data analysis strategy often consists in identifying both the big oppositions and special but very localized signatures. The latter are usually small (~1% reflectance) and localized in a few spectral channels and few spatial pixels. Since they are superimposed on large variations of albedo affecting all channels, they represent a very small share of the total variance and are difficult to evidence. Since modern space experiments generate very large datasets (~1Gb / day for several years), efficient automated data analysis techniques are now required to process these observations.

2. Data model

The signal measured on a planetary surface can be described as a linear mixture of the spectra of the main units (end-members), combined with uncorrected instrumental effects and noise. In this model, the endmembers are assumed to be representative of large units with common spectral properties covering at least some pixels at the surface. For this reason, endmembers are assumed to represent geological terrains and associations of minerals (rocks), not the mineral themselves which do not combine linearly at small scale. In the case of Mars or Titan, atmospheric signatures are also expected to contribute to the signal. This model can be written as:

$$D = AS + B$$

where D is the data array (N pixels × P channels), S are the endmembers (M spectral sources × P), A is the mixing coefficients matrix (N × M), and B is the noise. The spectra of the N pixels can be seen either as observables (physical point of view) or variables (statistical point of view).

Some tools have been extensively used to identify such end-member components in data cubes, in particular linear mixing methods and Principal Components Analysis (PCA). In these cases, the data cubes are reduced to simple 2D data arrays — the spectra are analyzed independently, with no consideration for spatial proximity between pixels. PCA is based on variance analysis and is easily applied to spectral cubes. However, PCA has long been known to provide limited-accuracy results in this context.

Conversely, ACI is aiming at identifying a set of statistically independent components, i.e., such that their marginal probability distribution functions are separable. This is done in three steps: first, the variables are decorrelated with a PCA; second, the array of the main M components is normalized (whitening step); third, the components are rotated

along the independent directions. Following the central limit theorem, this last step is performed by looking for the direction of maximum departure from Gaussianity. The remaining subspace is then analyzed similarly. A convenient algorithm for this step is JADE, which is based on joint diagonalization of the fourth order cumulant tensor. Because of the whitening step the resulting components are no longer constrained to be orthogonal in the variables space, which helps separating overlapping signatures. This is done at the expense of the knowledge of their sign and magnitude. JADE scales the components to unit variance, and order them according to the non-Gaussianity parameter, *i.e.*, to the level of heterogeneity they introduce in the dataset.

With both PCA and ICA, the spectral components allow the study of endmembers composition, while the coefficients can be mapped to estimate their spatial distribution.

4. Comparisons

Applications related to VIRTIS / Rosetta, VIRTIS / Venus-Express [1], OMEGA/Mars-Express [2,3], and adaptive optics observations of Mercury [4] and Ceres will be discussed.

Three major limitations often affect PCA results: 1) overlapping spectral features are not easily separated, because PCA looks for orthogonal components; 2) this situation is enforced when spectral parameters have similar variance, in which case they are not separated; 3) noise is never distinguished from signal, which commonly results in noisy components dominating more structured ones.

ICA does not present these limitations: separation of overlapping signatures or parameters of similar variance is more efficient because there is no orthogonality constraint; additive Gaussian noise is clearly separated from the signal, which makes ICA much more robust to random noise in this context. Altogether, the results of ICA are easier to interpret because independent components are closer to physical associations of variables than principal components, and minor signatures are more readily identified from the heterogeneity they introduce in a dataset.

References

[1] S. Erard, P. Drossart, and G. Piccioni (2009) Multivariate analysis of VIRTIS/Venus Express nightside and limb observations. JGR(Planets), vol. 114, E13.

[2] Forni et al. (2005) Component separation of OMEGA spectra with ICA. LPSC **XXXVI**, abstract #1623.

[3] Schmidt, F. et al. Implementation strategies for hyperspectral unmixing using Bayesian source separation, IEEE Transaction on Geoscience and Remote Sensing, 2010, 48, 4003-4013.

[4] Erard S., Bézard B., Doressoundiram A., Despan D. (2011) Mercury resolved spectroscopy from NTT. PSS **49**, 1842-1852.

EPSC Abstracts
Vol. 10, EPSC2015-463, 2015
European Planetary Science Congress 2015

Description of CoTCAT (Complement To CRISM Analysis Toolkit) and data reduction suite for CRISM

B. Bultel, C. Quantin and L. Lozac'h
Laboratoire de Géologie de Lyon: Terre, Planètes, Environnements, Université Lyon 1, ENS Lyon, CNRS UMR 5271, Villeurbanne, 2, rue Raphaël Dubois, 69622 Villeurbanne cedex, France. **Corresponding author:** Benjamin Bultel, +33472446235, benjamin.bultel@univ-lyon1.fr

Abstract

CRISM (Compact Reconnaissance Imaging Spectrometer for Mars) hyperspectral data have a spatial resolution ranging from 12 to 36m/pixel allowing the high resolution mapping of minerals at the surface of Mars. However, the signal-to-noise ratio (SNR) makes challenging the discrimination of minerals spectrally close such as certain phyllosilicates and carbonates. Here, we discuss different processing of data reduction used to improve the signal-to-noise ratio and to highlight the alteration minerals at the surface of Mars and their limit. We show that our tool allows to understand trends in global mineralogy present in hyperspectral data cube.

1. Introduction

CRISM on-board MRO (Mars Reconnaissance Orbiter) is a visible to near-infrared hyperspectral imaging spectrometer between 0.4-4.0 µm with a spectral resolution of 6.10^{-3} µm. We here use the Targeted Data mode that acquires data at spatial resolutions ranging from 12 to 36m/pixel. The S detector samples wavelengths from 0.4 to 1.0 µm (107 channels), and the L detector samples wavelengths from 1.0 to 4.0 µm (438 channels) [1]. The NIR domain is often used to detect the hydrated minerals on the surface as they have characteristic absorptions between 1.9 µm and 2.6 µm [1].

CAT (CRISM Analysis Toolkit) is a pipeline developed by the CRISM Team that allows the correction of the photometric effects, the atmosphere contribution and the first order noise [1, 2, 3 and 4]. Even after those processing, it is still challenging to discriminate different minerals with slight spectral difference like alteration mineral [5, 6 and 7]. We present a processing of data reduction to use as a complement of CAT to remove the noise still present in the data after the use of CAT. We present here this method and its tests on synthetic data cube built with artificially noised spectra from spectral library. We then applied ratioing method to highlight the main absorption present in the spectra. It allows us to use a trend tools to understand the global mineralogy present in the cube.

2. From CAT to CoTCAT

We use CAT to preprocess the CRISM data. It first applies a photometric correction [1]. Then, it corrects contribution of the atmosphere [2 and 3]. CAT also includes a filtering tool (CIRRUS: CRISM Iterative Recognition and Removal of Unwanted Spiking) that first remove the outlying values along the spectral dimension named as spectral spike [4]. The filtering tool also removes the spatial stripes by the median of neighbour values in the spatial dimension. Even after these processing, data are still noisy especially the ones acquired after several years around Mars and there is often a remaining spectral contribution of the Martian atmosphere.

We design a noise removal pipeline to be used after CAT preprocessing to denoised and smooth the data. It consists in the application of three successive filters: the sharpening-median filter, a mobile median and a mobile average filter [8]. The mobile average is used to smooth the signal, but this filter is sensitive to isolated value (spike). We so use a median filter before which is supposed to be less sensitive to isolated values. We start with a sharpening-median filter which function is to detect the isolated value and replace them. This filter is so the less sensitive to isolated values allowing afterwards the use of the mobile median and the mobile average.

3. Ratioing methods

The remnant contribution of atmosphere, the presence of dust and the existence of instrumental artifacts still bother the study of any CRISM cube. Ratioing methods are used to remove their contributions [1 and 6]. The most usual method is to use as denominator a spectrum judged by the user as spectrally neutral when possible in the same column

of detector as the target spectrum [6 and 9]. This method has the disadvantage to be manual and to possibly introduce a bias. We investigate different way of automatic ratioing method of a CRISM data cube. First, we analyze the use of the median spectrum of the whole data cube as denominator. Then, for comparison, we process to the automatic ratio of the data cube by the median spectrum of each column that is supposed to remove the detector dependent effects, or the smile effect [1]. In some case, the median spectrum on each column is not spectrally neutral. We so developed an automatic tool to search for the most spectrally neutral spectrum of each column of detector. On each column, the spectrum with the less variation of reflectance channel by channel is selected to be the denominator for the column.

A comparison of the different ratios allows us to conclude that they are all efficient to highlight alteration minerals but that their use for interpretation of the global shape of the spectrum may by strongly affected by the shape of the denominator [1] while it may be more challenging for mafic mineral that have efficient way to highlight the surface.

4. Trend tool

Alteration minerals such as phyllosilicates carbonates, zeolithes, ferric oxydes, mono- and poluyhydrated sulfates have different diagnostic combinations of absorptions. We built a tool that (1) can found the two main absorptions on all the spectra of a CRISM cube; (2) remove the continuum and (3) determine the exact centres of absorptions. The results are plot in a graphic that discriminate different mineral phase.

It allows us to understand trends in global mineralogy present in the cube studied. This tool is not claiming to conclude on the mineralogy present in a data cube but is a powerful guideline for the spectral analysis.

4. Discussion and conclusion

The denoising tools, the ratioing methods and the data reduction tool present have been tested on library spectra artificially noised and on CRISM data, these results will be presented. We suggest here a simple tool of noise removal to be used as a complement to others noise removal techniques. Our tests reveal the relevance of our tools until SNR as low as 20. We have compared the analyze of CRISM data cube with and without our complement tools. We have demonstrated that the use of our tools greatly improves the mineral mapping technique using band depth map computation but that quantitative data processing must be carried out with care due to the decrease of the spectral fidelity. This tool could be a valuable support to Martian local geological investigation such the ones required for the landing sites selection of robotic missions.

Acknowledgements

The research leading to these results has received funding from the European Research Council under the European Union's Seventh Framework Program (FP7/2007-2013)/ERC Grant agreement n° 280168.

References

[1] Murchie, S., et al. (2007), Compact Reconnaissance Imaging Spectrometer for Mars (CRISM) on Mars Reconnaissance Orbiter (MRO), J. Geophys. Res., 112, E05S03.

[2] Langevin et al., 2005b, Summer Evolution of the North Polar Cap of Mars as Observed by OMEGA/Mars Express, Science, Vol. 307, p. 1581-1584.

[3] McGuire et al., 2008, An improvement to the volcano-scan algorithm for atmospheric correction of CRISM and OMEGA spectral data, Transactions on geoscience and remote sensing, Vol. 46 Issue 12 p. 4020-4040.

[4] Parente, M., 2008, Denoising CRISM images: a new look, LPSC 39, #1391.

[5] D'Agostino, R. B. and Stephens, M. A., 1986. Goodness-of-Fit Techniques, Marcel Dekker, Inc., New York. Chapter 12

[6] Ehlmann, B. L., et al. (2009), Identification of hydrated silicate minerals on Mars using MRO-CRISM: Geologic context near Nili Fossae and implications for aqueous alteration, J. Geophys. Res., 114.

[7] Bultel et al., 2013, A new CRISM data analysis tool for the detection of miscellaneous alteration phases, EPSC2013

[8] Bultel et al., (2015), Description of CoTCAT (Complement to CRISM Analysis Toolkit), IEEE Journal Of Selected Topics In Applied Earth Observations And Remote Sensing

[9] Carter, J. et al., (2013), Hydrous minerals on Mars as seen by the CRISM and OMEGA imaging spectrometers: Updated global view, J. Geophys. Res. Planets, 118.

EPSC Abstracts
Vol. 10, EPSC2015-576, 2015
European Planetary Science Congress 2015

Online spectral fit tool (OSFT) for analyzing reflectance spectra

A. Penttilä (1), T. Kohout (1) and K. Muinonen (1,2)
(1) University of Helsinki, Finland, (2) Finnish Geospatial Research Institute (Antti.I.Penttila@helsinki.fi)

Abstract

We present an algorithm and its implementation for fitting continuum and absorption bands to UV/VIS/NIR reflectance spectra. The implementation is done completely in JavaScript and HTML, and will run in any modern web browser without requiring external libraries to be installed.

1. Introduction

The Online Spectral Fit Tool (OSFT) [1] was developed to our own needs in analyzing VIS-NIR spectral behavior of asteroids and meteorites. Our approach is similar to the Modified Gaussian Model (MGM) - software by Sunshine et al. [2, 3], but with certain differences in the model and in the implementation. We extended the applicability of our software by implementing it in JavaScript/HTML so that it can be used through a web browser. The OSFT runs in the client-side, and is self-consistent needing no plug-ins to be installed. The OSFT uses two public third-party JavaScript libraries [4, 5] included in the software.

We use no pre-determined spectral data, but fit the spectra using mathematical continuum model and analytical functions for absorption bands. The OSFT does not relate the fit directly to known spectral elements, but gives statistics describing the behavior of the continuum and the absorption bands. There are some semi-physical assumptions behind the MGM model. However, some of them are quite approximate when it comes to reflectance spectra of solid mineral samples. With the Central Limit Theorem, one can vaguely justify the Gaussian distribution as a model for an absorption band arising from several overlapping effects. On the other hand, also the Lorentzian band shape (i.e., Cauchy distribution) is used. Sunshine et al. [2] justify using the modified Gaussian model by crystal field theory and empirical tests. We feel that any of the abovementioned band shapes are not, strictly speaking, derived directly from physical principles applicable to mineral reflectance. Thus, we choose to use a band model that seems to fit best to our data.

2. OSFT Model Formulation

Our model for UV-VIS-NIR spectra is based on continuum with superimposed absorption bands. The model parameters are fitted using constrained non-linear optimization.

2.1. Absorption bands

We use the shape of the Gamma distribution for the absorption bands. The Gamma shape seems to fit the data better than the Gaussian, Lorentzian or modified Gaussian shape. The Gamma distribution is more peaked than the Gaussian, and is favored by our data. The distribution is defined for positive values, supporting its use with wavelengths. If the expected value μ of the Gamma distribution is large, i.e., $\mu/\sigma \gg 0$, the distribution is almost symmetric. We use an alternative parameterization of the distribution where μ and the standard deviation σ are the parameters of the distribution. The probability density function f is

$$f(x;\mu,\sigma) = \frac{1}{x\,\Gamma\left(\frac{\mu^2}{\sigma^2}\right)}\, e^{-\frac{\mu x}{\sigma^2}} \left(\frac{\sigma^2}{\mu x}\right)^{-\frac{\mu^2}{\sigma^2}}, \qquad (1)$$

where Γ is the Gamma function and $x > 0$. The actual absorption peak p in the model is the normalized Gamma distribution to have maximum value of 1[1], and multiplied by the peak strength parameter c:

$$p(x;\mu,\sigma,c) = \frac{c}{f(\mu;\mu,\sigma)}\, f(x;\mu,\sigma). \qquad (2)$$

The area A of the band can be derived analytically:

$$\begin{aligned} A(\mu,\sigma,c) &= \int_0^\infty p(x;\mu,\sigma,c)\,dx \\ &= c\, e^{\frac{\mu^2}{\sigma^2}}\, \mu \left(\frac{\mu}{\sigma}\right)^{-\frac{2\mu^2}{\sigma^2}} \Gamma\left(\frac{\mu^2}{\sigma^2}\right), \end{aligned} \qquad (3)$$

[1] Approximately. Because the distribution is not strictly symmetric, $f(\mu;\mu,\sigma)$ can be slightly smaller than the maximum value of the distribution.

while the full-width-at-half-max (FWHM) w of the peak needs to be solved numerically by finding x's.

2.2. Continuum

We wanted the continuum model to be more flexible than the first-order polynomials. For this reason, we chose cubic splines as the basis of the continuum. The continuum is modeled as the linear combination of five B-spline basis functions of third degree with knots in the range from the smallest wavelength λ_{min} to the largest wavelength λ_{max} in the data. The coefficients b_i of the linear combination are to be fitted.

2.3. Fit

The final fit $g(\lambda)$ to the data is:

$$g(\lambda) = \sum_{i=0}^{4} b_i s_i(\lambda) - \sum_{i=1}^{n} p(\lambda; \mu_i, \sigma_i, c_i), \quad (4)$$

where s_i are the ith B-splines of degree 3, λ is the wavelength, n is the number of absorption peaks, and μ_i, σ_i, c_i are the mean, standard deviation, and depth for peak i.

2.4. Optimization

The function $g(\lambda)$ is fitted to the data using constrained non-linear optimization. The sum-of-squared-errors (SSE) between the data and the model is minimized. Constraints need to be set for the band parameters. All standard deviations and depth parameters $\sigma_i, c_i \geq 0$. The mean parameters need to be ordered, $\lambda_{min} \leq \mu_1 \leq \cdots \leq \mu_n \leq \lambda_{max}$. Actually, in addition to minimizing SSE, we also introduce two other penalizations with small weights. These penalizations are related to the continuum being smooth and the bands to extend only to the area of absorption and not to continuum.

3. Usage

The beta version of the OSFT is publicly available [1]. The user can upload a text-file of wavelength-reflectance pairs. The data is shown graphically, and the user can select the number of absorption bands. Initial parameter guesses need to be given for band centers, deviations, and depths. With initial values for bands, the continuum is fitted using the linear least-squares fit, and the initial fit is displayed with the data. Once the initial fit is in the right neighborhood, the algorithm will do the actual non-linear fit for the band and continuum parameters together. When completed, the software can compute fit statistics, i.e., band locations, deviations, depths, FWHM-values, and band areas, together with the slope and albedo parameters. At this point, the data can also be normalized at a given wavelength. We prefer to normalize only after the fitting, since we rather normalize with the value from the fitted continuum than with a single measured reflectance value. A single measured value can contain errors which will affect the slope and band depths, while the fitted continuum is 'an average' and thus have smaller errors. Fig. 1 shows two examples of the fit produced by the OSFT.

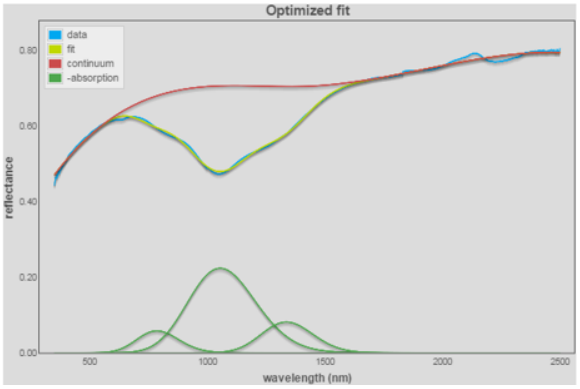

Figure 1: OSFT fit with three overlapping absorption bands for olivine including nanophase Fe^0.

Acknowledgements

AP and KM acknowledge the ERC Advanced Grant No. 320773, Scattering and Absorption of Electromagnetic Waves in Particulate Media (SAEMPL).

References

[1] A. Penttilä and T. Kohout (2015). OSFT tool, http://www.helsinki.fi/project/psr/OSFT/.

[2] J.M. Sunshine, C.M. Pieters, and S.F. Pratt (1990). JGR 95, 6955–6966.

[3] J.M. Sunshine, C.M. Pieters, S.F. Pratt, and K.S. McNaron-Brown (1999). Abstract, LPSC 30.

[4] A. Gustafsson (2012). Cobyla2 port to JavaScript, http://code.google.com/p/jscobyla/.

[5] Flotr2 Canvas graphing library (2014), http://www.humblesoftware.com/flotr2/.

EPSC Abstracts
Vol. 10, EPSC2015-629, 2015
European Planetary Science Congress 2015

Investigating the composition of Potentially Hazardous Asteroids with the NEO-SURFACE survey

S. Ieva (1), E. Dotto (1), D. Perna (2), M.A. Barucci (2), F. Bernardi (3), E. Perozzi (4,5,6), M. Micheli (3,5,6), E. Mazzotta Epifani (1), J.R. Brucato (7), S. Fornasier (2), F. De Luise (8), A. Rossi (9)

(1) INAF - Oss. Astr. Roma, I (simone.ieva@oa-roma.inaf.it), (2) LESIA - Obs. Paris, F, (3) SpaceDyS, I, (4) Deimos Space, RO, (5) INAF – IAPS, I, (6) ESA NEOCC, I, (7) INAF - Oss. Astr. Arcetri, I, (8) INAF – Oss. Astr. Teramo, I, (9) IFAC – CNR, I (simone.ieva@oa-roma.inaf.it)

Abstract

There is a high degree of diversity among the physical properties of the Potentially Hazardous asteroids (PHAs). For these objects, the physical characterization is essential to define a successful mitigation mission, therefore ground-based surveys like NEO-SURFACE could provide a fundamental contribution. Our analysis suggest a prevalence of silicate S-types in the PHA population, which could be due in principle to the high efficiency of the transport mechanisms in the inner main belt, or to an observational bias due to the fact that S-types are brighter.

1. Introduction

There is a great diversity among the physical characteristics of Potentially Hazardous Asteroids (PHAs), a class of Near-Earth Asteroids (NEAs) that deserve special attention due to the risk they pose to our planet. PHAs have compositions ranging from siliceous to carbonaceous, from basaltic to metallic, implying also completely different internal densities and strengths [1].
Physical characterization for these objects is essential to define successful mitigation strategies in case of possible impacts. In fact, whatever the scenario, it is clear that the technology needed to set up a realistic mitigation strategy strongly depends upon the knowledge of the physical properties of the impacting object. The analysis of its surface characteristics, which are connected with the internal structure, is an essential step towards developing means of deflection or destruction of the object. Unfortunately, our knowledge of the physical nature of PHAs is still rather limited, since almost 85% of the known PHAs do not have spectral types determined from observations. Several of them are large (D > 1 km) asteroids.
In order to increase the present knowledge of the physical properties of PHAs and NEAs easily accessible for a rendez-vous space mission we are carrying out a survey called NEO-SURFACE: Near Earth Objects - SURvey oF Asteroids Close to the Earth [2].

2. Observations and results

Data here presented have been collected in three different runs (December 2012, July and August 2014) at the Telescopio Nazionale Galileo (TNG) located at the Roque de los Muchachos Observatory in La Palma, Canary Islands, using the DOLORES detector (Device Optimised for the LOw RESolution) in photometric and spectroscopic mode.
We observed a global sample of 21 PHAs. We combined our visible spectra with infrared data, when available, from the MIT spectral catalogue [3] to constrain the taxonomic classification and identify a suitable meteorite analogue class for each observed PHA. Sixteen asteroids were classified as belonging to the S-complex, while only three PHAs were classified as belonging to the C-complex. Nineteen of these objects were taxonomically classified for the first time.

3. Conclusions

Considering the global sample of 255 PHAs with some physical characterization [5] (Fig. 1) there is a prevalence of silicate S-types over more porous carbonaceous C-types. This is probably due to dynamical effects, since S-types are more common in the inner main belt and they are closer to the 3:1 mean motion resonance with Jupiter, which pump

their eccentricity and push hem into near-Earth orbits.

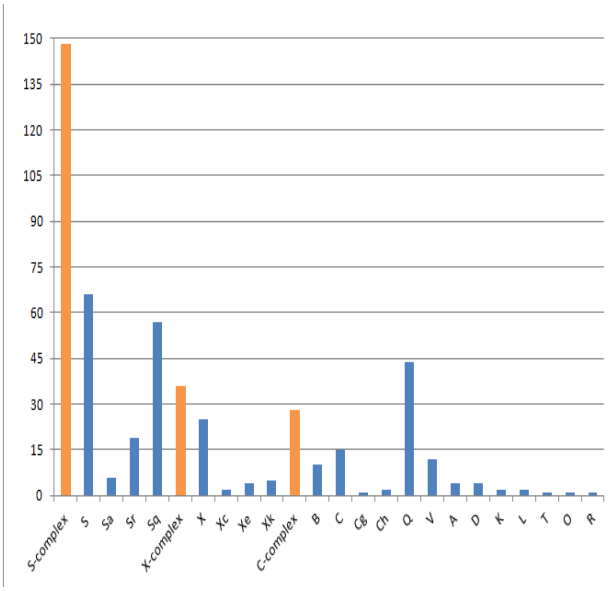

Figure 1 : The distribution of taxonomic classes among the sample of 255+19 PHAs with physical characterization.

However an observational bias, due to the fact that S-types are brighter, cannot be excluded [4]. Ground-based surveys, like NEO-SURFACE, can increase the number of PHAs with physical characterization, and likely provide a fundamental contribution to this purpose.

C-types are also the most interesting targets for a sample-return mission, since they contain pristine material and organic, prebiotic compounds. For this kind of mission ground-based surveys are crucial to guarantee the technical feasibility and the high scientific return, since the cost is extremely elevated and it depends on the orbit of the chosen object.

References

[1] Binzel, R., Rivkin, A., Stuart, J. et al. 2004, Icarus 170, 259

[2] www.oa-roma.inaf.it/planet/NEOSurface.html

[3] http://smass.mit.edu/catalog.php

[4] Mainzer, A., Bauer, J., Grav, T. et al. 2014, ApJ 784, 110

[5] http://earn.dlr.de/nea/table1_new.html

EPSC Abstracts
Vol. 10, EPSC2015-676, 2015
European Planetary Science Congress 2015

Multi-angle Approach for Coherent Retrieval of Surface Reflectance and Atmosphere Optical Depth from CRISM Observations

S. Douté (1) and X. Ceamanos (2)
(1) Institut de Planétologie et d'Astrophysique de Grenoble (IPAG), UJF-CNRS, UMR 5274, 38041 Grenoble. (e-mail: sylvain.doute@obs. ujf-grenoble.fr), (2) DOTA/POS ONERA Toulouse, France.

Abstract

This paper addresses the correction for aerosol effects in near-simultaneous multi-angle observations acquired by the Compact Reconnaissance Imaging Spectrometer for Mars (CRISM) aboard the Mars Reconnaissance Orbiter. In the targeted mode, CRISM senses planet Mars from the top of the atmosphere (TOA) using 11 viewing angles in 437 visible and infrared wavelengths, which allow it to provide unique information on the scattering properties of surface materials and atmospheric aerosols. In order to retrieve these data, however, appropriate strategies must be used to model the signal sensed by CRISM and compensate for aerosol contribution. In [2] we put forward an innovative inversion scheme of the model named Multi-angle Approach for Retrieval of Surface Reflectance from CRISM Observations (MARS-ReCO). Nevertheless this first version of MARS-ReCO requires a priori information about the scattering properties and the abundance of the atmospheric aerosols prior to the inversion. The proposed method retrieves conjointly the atmosphere optical depth (AOD) and the bidirectional reflectance factor (BRF) of surface materials as a function of wavelength. MARS-ReCO represents a substantial improvement regarding previous techniques as it takes into consideration in a coherent way the anisotropy of both the surface and the atmosphere scattering. Thus it provides more realistic surface and atmospheric products. Furthermore, MARS-ReCO is fast and provides error bars on the retrieved parameters.

1. Method

MARS-ReCO performs the atmospheric correction of each TOA photometric curve $\mathbf{R}^C = \left\{R^C_1, \ldots, R^C_{Ng}\right\}$ extracted from a targeted observation where Ng is the number of available angular measurements. Following [3] signal sensed by CRISM can be decomposed as a sum of the atmospheric path radiance (D), and the radiance reflected by the surface before being directly ($L_s e^{-\tau_0/|\mu|}$) and diffusely (L^d_s) transmitted through the atmosphere. The surface anisotropy is taken into account through its BRF expressed using a semi-empirical Ross-Thick Li-Sparse (RTLS) model:

$$\rho\left(\mu_0,\mu,\varphi\right) = k^L + k^G f_G\left(\mu_0,\mu,\varphi\right) + k^V f_V\left(\mu_0,\mu,\varphi\right) \quad (1)$$

The subscripts refer to Lambertian (L), geometric (G) and volumetric (V) components with f_G and f_V predefined geometric kernels. The substitution of the RTLS model into the surface-atmosphere radiative transfer scheme provides a quasi-linear expression for the TOA signal : a linear combination of kernels.

$$\begin{aligned} R\left(\mu_o,\mu,\varphi\right) &= R^D\left(\mu_o,\mu,\varphi\right) + k^L F^L\left(\mu_o,\mu\right) + k^G F^G(\\ &\quad + k^V F^V\left(\mu_o,\mu,\varphi\right) + R^{nl}\left(\mu_o,\mu\right) \end{aligned}$$

The kernels $\left\{F^L, F^G, F^V\right\}$, the path radiance R^D, and the surface dependent nonlinear term R^{nl} can be conveniently stored in reference look-up tables. In [1], assuming the AOD is known, an iterative inversion strategy of the TOA model is proposed based on an unconstrained linear inversion procedure. The method we propose in present paper is based on the evolution of the previous scheme with the AOD now a free parameter. Since our model of the TOA radiance already contains an additive atmospheric term in addition to the linear combination of surface kernels, we can define an atmospheric kernel which linear coefficient is the AOD. $R^D\left(\mu_o,\mu,\varphi\right) = k^T F^T\left(\mu_o,\mu,\varphi\right)$ where $F^T\left(\mu_o,\mu,\varphi\right) = R^D\left(\mu_o,\mu,\varphi\right)/k^T$. Then we have a pseudo linear model relating (k_L, k_G, k_V, k_T) with the vector of the observables. A first guess for the AOD, which is assimilated to k_T, allows to calculate the atmospheric kernel F^T. The latter is refined iteration after iteration along with the solution for k_T.

Second we borrow a Kalman filter based method presented by [2]. We adapt this procedure to the processing of multi-angle CRISM data in order to enhance the robustness of the inversion since our model, with 3 surface and one atmosphere free parameters, is not well constrained. We consider that the atmosphere opacity is usually more stationary than the properties of the martian surface in the spatial dimension because of the reduced size of the CRISM scenes (15x15 km). Thus the spatial dimension is exploited for simultaneous retrieval of the surface BRF and AOT. The solution is obtained through the unconstrained linear inversion procedure but perpetuated in space using a Kalman filter. Practically the solution k_{sol} and a posteriori covariance matrices $\mathbf{C}_{kp}$ for pixel $J-1$ are used to calculate a prior C_x and k_p for super-pixel J according to a prognostic model operator:

$$k_p = k_{sol} \tag{4}$$

$$C_x = (1+\delta)\mathrm{diag}(\mathrm{C_{kp}}) \tag{5}$$

The transition probabilities for the variances are described by vector :

$$\delta = \left(2^{2/t_1}-1,\ 2^{2/t_2}-1,\ 2^{2/t_3}-1,\ 2^{2/t_4}-1\right) \tag{6}$$

Then the iterative inversion scheme described above is applied to super-pixel J with the following regularized first guess and a priori covariance matrix:

$$C_k = \left(C_x^{-1} + C_{reg}^{-1}\right)^{-1} \tag{7}$$

$$k^{(0)} = C_k\left(C_x^{-1}k_p + C_{reg}^{-1}k_{reg}\right) \tag{8}$$

C_{reg} and k_{reg} are respectively a fixed regularization matrix and vector. One must note that the retrieval of the RTLS kernel weights and AOD by the previous scheme with two nested iterative loops is performed independently for each wavelength.

2. Numerical experiments and results

Validation of our method has been performed on a selection of 40 CRISM observations with different surface, atmospheric, and geometrical conditions. The chosen characteristic "times" (going from one pixel to the next) for the Kalman transition are t1=2; t2=10; t3=10 for the surface model and is variable for the AOD (a decreasing function of the number of valid CRISM geometries). For each observation, we assess the quality of the solution generated by MARS-ReCO by considering the behavior kT in the spatial and spectral dimensions (Fig. 1). First we have at a wavelength of 1.1 micron the evolution of the AOD as a function of the pixel sequence number in the inversion spatial path through the scene. This evolution allows us to estimate the quality of the convergence since the optical thickness should be spatially homogeneous in most cases. Second we consider the kT spectra of a series of pixels to assess the mean spectral dependance of tau as well as the variance around this mean. Note that the mean spectral slope is indicative of the aerosol size distribution. Based on a compilation of the obtained results for the selection of CRISM observations we conclude that the algorithm produces very satisfactory results except when the phase angle range is limited, the incidence angle is higher than 70, the topography is accuentuated or perhaps a combination of these three factors.

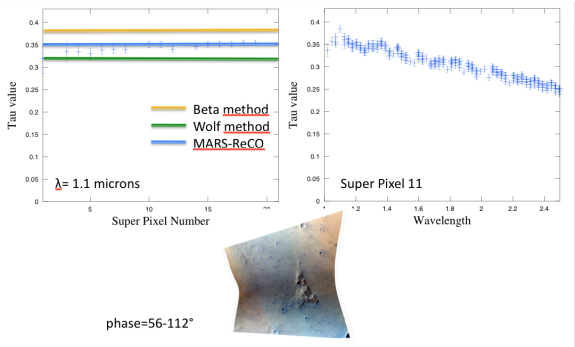

Figure 1: Behavior of the AOD solution as a function of the pixel sequence number and of the wavelength. For observation FRT3192 convergence of the MARS-ReCO algorithm is very satisfactory and the dispersion of the k_T spectra is weak.

Acknowledgements

This work is supported by a contract with PNTS and ANR.

References

[1] D. Carreret al., Journal of Geophysical Research (Atmospheres), vol. 115, pp. 10208, May 2010.

[2] X. Ceamanos et al., Journal of Geophysical Research (Planets), vol. 118, pp. 1–20, 2013.

[3] A. Lyapustin and Y. Knyazikhin, Applied Optics, vol. 40, pp. 3495–3501, July 2001.

EPSC Abstracts
Vol. 10, EPSC2015-701, 2015
European Planetary Science Congress 2015

Light-scattering simulations of space-weathering effects on asteroid and meteorite spectra

A. Penttilä (1), T. Väisänen (1), J. Martikainen (1), T. Kohout (1) and K. Muinonen (1,2)
(1) University of Helsinki, Finland, (2) Finnish Geospatial Research Institute (Antti.I.Penttila@helsinki.fi)

Abstract

We present results of numerical light-scattering modeling for the measured VIS-NIR spectra of olivine. The space-weathering effects with nanophase iron inclusions are experimentally introduced to the olivine matrix, and modeled in the radiative-transfer simulations. A good agreement between the measured and the modeled spectra is found.

1. Space-weathering in laboratory samples

Space weathering introduces changes to the reflectance spectra of asteroid surfaces. In silicate minerals, space weathering is known to darken the spectra, reduce the silicate absorption band depths, and increase the spectral positive slope in visual and near-infrared wavelengths (see, e.g., [1], and references therein).

The space-weathering process is believed to influence the spectra by generating small nanophase iron ($npFe^0$) inclusions in the surface layers of mineral grains (see Fig. 1). The $npFe^0$ inclusions are believed to be one to some tens of nanometers in size. This mechanism has been linked to the Moon and to a certain extent also to the silicate-rich S-complex asteroids and to the ordinary chondrite meteorites.

Kohout et al. [1] have experimentally treated pure olivine powder to simulate the space-weathering effects. They have measured the VIS-NIR spectra of the powder consisting of untreated olivine, and olivine with various degrees of nanophase iron inclusions, see Fig. 1. In this work, we will model the spectral changes with light-scattering computations.

2. Radiative-transfer simulations

We will present light-scattering simulations that validate the space-weathering and $npFe^0$ effects on the spectra of olivine. All the observed effects, i.e., the darkening and reddening of the spectra, as well as the flattening of the 1-μm absorption band, can be reproduced in the simulations. We use a radiative-transfer solution and the implementation by Muinonen et al. [2], the so-called SIRIS code. The code can treat surface and internal reflections by a random-shaped particle (i.e., olivine grain) that can include internal diffuse scatterers (i.e., nanophase iron inclusions), and compute the reflectance spectra over varying wavelengths. Laboratory-measured, wavelength-dependent complex refractive indices of olivine and iron are used in the model as input. The resulting spectra reproduces the observed space-weathering effects, see Fig. 2. This result is important in understanding the observed spectral space-weathering effects using the light-scattering theory.

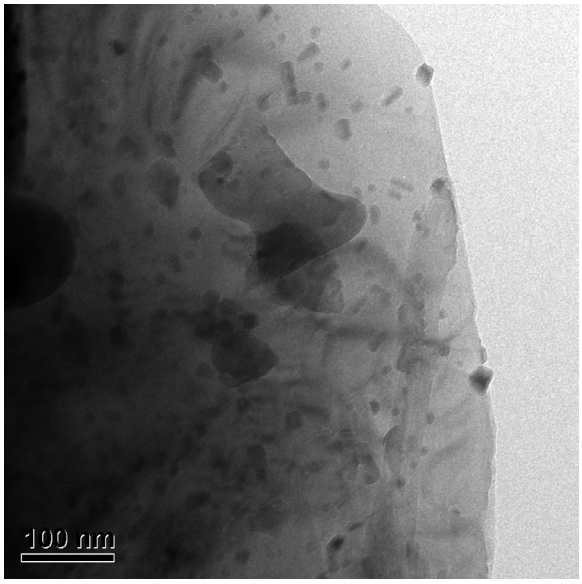

Figure 1: TEM image, originally published in [1], of nanoparticles on olivine powder grains. Two populations can be observed (∼5–20 nm and ∼40–50 nm).

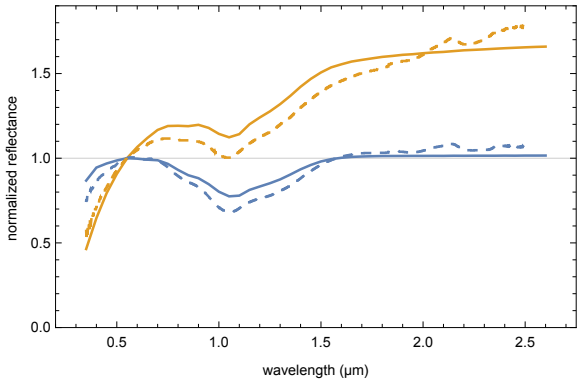

Figure 2: Measured and simulated normalized reflectance spectra of untreated and space-weathered olivine. The solid lines present the simulations, and the dashed lines the measurements. The blue lines are for the untreated olivine grains, and the orange lines for olivine with nanophase iron (0.023 wt%).

Acknowledgements

KM and AP acknowledge the ERC Advanced Grant No. 320773, Scattering and Absorption of Electromagnetic Waves in Particulate Media (SAEMPL). Computations are partly done using the resources provided by the CSC — The IT Center For Science, Finland.

References

[1] T. Kohout, J. Čuda, J. Filip, D. Britt, T. Bradley, J. Tuček, R. Skála, G. Kletetschka, J. Kašlík, O. Malina, K. Šišková, R. Zbořil (2014). Space weathering simulations through controlled growth of iron nanoparticles on olivine. Icarus 237, 75–83.

[2] K. Muinonen, T. Nousiainen, H. Lindqvist, O. Muñoz, G. Videen (2009). Light scattering by Gaussian particles with internal inclusions and roughened surfaces using ray optics. Journal of Quantitative Spectroscopy & Radiative Transfer 110, 1628–1639.